Chinese Chemical Letters 36 (2025) 109786

Contents lists available at ScienceDirect

Chinese Chemical Letters

journal homepage: www.elsevier.com/locate/cclet

"Superimposed" spectral characteristics of fluorophores arising from cross-conjugation hybridization

Kai An[a,b], Qinglong Qiao[a], Lovelesh[c], Syed Ali Abbas Abedi[c], Xiaogang Liu[c,*], Zhaochao Xu[a,b,*]

[a] CAS Key Laboratory of Separation Science for Analytical Chemistry, Dalian Institute of Chemical Physics, Chinese Academy of Sciences, Dalian 116023, China
[b] University of Chinese Academy of Sciences, Beijing 100049, China
[c] Fluorescence Research Group, Singapore University of Technology and Design, Singapore 487372, Singapore

ARTICLE INFO

Article history:
Received 10 March 2024
Revised 15 March 2024
Accepted 18 March 2024
Available online 18 March 2024

Keywords:
Fluorophore
Cross conjugation
Absorption
Emission
Naphthalene

ABSTRACT

The demand for enhanced optical properties in advanced fluorescence technologies has driven research into the structure-property relationship of fluorophores. In this paper, we use naphthalene fluorophores **NaDC-Aze** and **PhDO-Aze** as a case study to emphasize the pivotal role of cross conjugation in tuning the optical structure-property relationship. **NaDC-Aze** and **PhDO-Aze**, formed by hybridizing two distinct conjugated systems in a single naphthalene molecule, exhibit spectral characteristics from both conjugated systems. Experimental data and theoretical calculations demonstrate the coexistence of two electron-delocalization systems in a cross-conjugation manner in both **NaDC-Aze** and **PhDO-Aze**. The cross-conjugation fluorophores exhibit high brightness, large Stokes shift, and a broad absorption wavelength range by combining distinct spectral properties from its parent fluorophores. These spectral properties will be advantageous for certain applications (*i.e.*, panchromatic absorption in organic solar cells, and fluorophores compatible with a wide range of excitation wavelengths).

Studies on the fluorescence principle have continuously progressed, culminating in the current molecular fluorescence theories that employ molecular structure to comprehend fluorescence properties [1,2]. The initial theory to comprehend such structure-property relationship of fluorophores breaks down fluorescent dyes or fluorophores into chromophore and auxochromophore components [3,4]. Subsequently, as valence bond theory progressed, it further advanced into the concept of conjugated/delocalized systems and the incorporation of electron-donating and electron-withdrawing groups [5–8]. The advent of frontier molecular orbital theory and its success in elucidating the optical properties of fluorophores placed further emphasis on the electronic structures of the fluorophores, in addition to their molecular structures [9,10]. Although our grasp of the structure-property relationship in organic fluorophores has advanced significantly, our ability to precisely tune the optical properties of these fluorophores remains constrained.

In recent years, advancements in fluorescence technology have revitalized the ancient research field of fluorescent dyes [11,12]. Innovations such as single-molecule and super-resolution fluorescence imaging [13,14], fluorescence-guided surgery [15], photodynamic [16], and photothermal [17] therapies have garnered significant attention. This resurgence in vigorous research necessitates a deeper understanding of fluorophore structures to achieve enhanced optical properties [10,18-21]. Consequently, there is an urgent need for breakthroughs in the understanding of fluorophores' structure-property relationships.

Cross-conjugation refers to a molecular arrangement in which alternating single and multiple bonds do not form a continuous conjugated system but are interrupted by non-conjugated groups or atoms. Cross conjugation in fluorophores involves the extension of conjugated systems across multiple branches or nonadjacent positions, alternating electronic communication [22]. The presence of multiple pathways for electron delocalization contributes to altered energy levels and electronic transitions, consequently influencing the absorption and emission properties [23]. However, there have been very few studies exploring cross-conjugation in fluorophores and their impact on optical properties.

In this paper, we use naphthalene fluorophores as a case study to explore the role of cross-conjugation in the optical structure-property relationship (Scheme 1). Electron-donating groups and electron-withdrawing groups are introduced at both ends of naphthalene (Scheme 1a). This arrangement induces intramolecular

* Corresponding authors.
E-mail addresses: xiaogang_liu@sutd.edu.sg (X. Liu), zcxu@dicp.ac.cn (Z. Xu).

https://doi.org/10.1016/j.cclet.2024.109786
1001-8417/

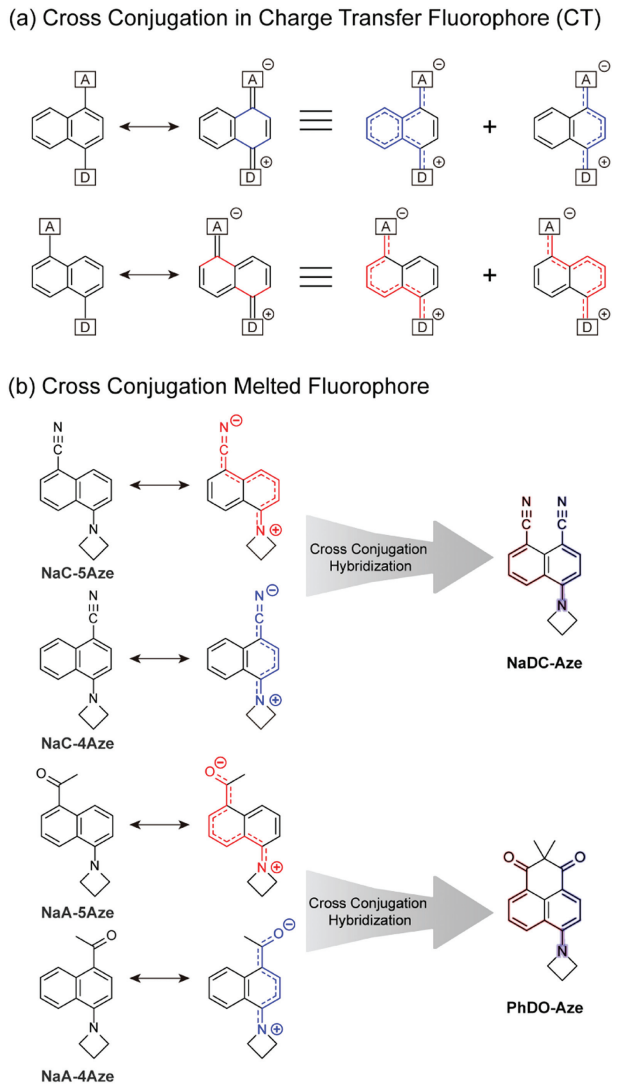

Scheme 1. Cross-conjugation in the optical structure-property relationship. (a) Cross-conjugation in charge-transfer (CT) fluorophore. (b) The structures of CT fluorophore and hybrid cross-conjugation fluorophores.

charge transfer, leading to the presence of the charge-separated quinone structure as one of the representative resonance hybrid structures (conjugated systems marked in blue and red, respectively, in Scheme 1a). Such fluorophores characterized by strong intramolecular charge transfer are termed charge-transfer fluorophores. When the position of the substituent changes, the conjugation pathways, and the associated cross-conjugation also change accordingly. As shown in Scheme 1b, we incorporated azetidine as an electron-donating group at one end of the naphthalene ring and introduced either a cyano group or an acetyl group as an electron-withdrawing group at different positions on the opposite end. This resulted in the formation of **NaC-5Aze** and **NaC-4Aze**, as well as **NaA-5Aze** and **NaA-4Aze**. These fluorophores are future hybridized to yield **NaDC-Aze** and **PhDO-Aze**, respectively. By theoretically analyzing the relationship between the spectral properties of **NaDC-Aze** and **PhDO-Aze** and their parent fluorophores **NaC-5Aze**/**NaC-4Aze** and **NaA-5Aze**/**NaA-4Aze**, we demonstrate that cross conjugation in fluorophores significantly influences absorption and emission properties.

We first examined the ultraviolet–visible (UV–vis) absorption and fluorescence spectra of these 6 compounds in 10 solvents (Tables 1 and 2; Fig. S1 and Tables S1–S4 in Supporting information). For the sake of simplicity, we chose to compare their spectra in DMSO within the main text (Fig. 1). The spectra vary significantly based on the different positions of the electron-withdrawing groups. Compounds **NaC-5Aze** and **NaA-5Aze**, featuring electron-donating and electron-withdrawing groups positioned at both ends of distinct benzene rings, exhibit noticeable redshifts in their maximum absorption and fluorescence wavelengths as the solvent polarity increases. In contrast, compounds **NaC-4Aze** and **NaA-4Aze**, where the electron-donating and electron-withdrawing groups are situated at both ends of the same benzene ring, exhibit small variations in the maximum absorption and fluorescence wavelengths as a function of solvent polarity. This distinction arises from the greater intramolecular charge transfer experienced by **NaC-5Aze** and **NaA-5Aze** upon light excitation, than that in **NaC-4Aze** and **NaA-4Aze**. The significant differences in intramolecular charge transfer also lead to disparate spectral properties. For example, the molar extinction coefficients of **NaC-5Aze** and **NaA-5Aze** are only approximately one-quarter of those in **NaC-4Aze** and **NaA-4Aze**. Additionally, the first absorption bands of **NaC-5Aze** and **NaA-5Aze** are of significantly longer wavelengths than those of **NaC-4Aze** and **NaA-4Aze**. Furthermore, **NaC-5Aze** and **NaA-5Aze** exhibit large Stokes shifts (170 and 270 nm in DMSO), while **NaC-4Aze** and **NaA-4Aze** demonstrate smaller Stokes shifts (60 and 50 nm in DMSO).

Fascinatingly, **NaDC-Aze** and **PhDO-Aze** exhibit spectral properties reminiscent of their parent dyes. Both **NaDC-Aze** and **PhDO-Aze** display two adjacent absorption peaks, with the wavelengths aligning with the absorption peaks of their two parent dyes (Fig. 1). The molar extinction coefficient falls between the absorption intensities of the two parent dyes as well. Furthermore, the maximum emission wavelength and Stokes shift of **NaDC-Aze** and **PhDO-Aze** also fall between the maximum emission wavelengths

Table 1
Photophysical data for **NaDC-Aze** in various solvents: peak UV–vis absorption wavelength (λ_{abs}), full width at half maximum ($FWHM_{abs}$) and peak area ($Area_{abs}$) in UV–vis spectra, maximum emission wavelength (λ_{em}), Stokes shifts ($\Delta\lambda$), molar absorption coefficients (ε) and fluorescence quantum yields (φ).

Solvent	λ_{abs}/nm	$FWHW_{abs}$/nm	$Area_{abs}$	λ_{em}/nm	$\Delta\lambda$/nm	φ	ε/L mol^{-1} cm^{-1}
Toluene	394	76	3.36	476	82	0.59	8746
$CHCl_3$	397	84	4.43	478	81	0.65	10,458
DCM	397	67	3.53	485	88	0.75	9268
EA	395	75	3.34	487	92	0.54	8588
ACN	399	69	3.32	503	104	0.57	8596
DMF	404	68	3.13	503	99	0.72	8158
DMSO	410	71	3.80	511	101	0.75	8992
EtOH	399	66	3.00	503	104	0.67	8162
MeOH	400	65	3.03	510	110	0.62	8382
H_2O	396	98	3.21	538	142	0.38	6974

Table 2
Photophysical data for **PhDO-Aze** in various solvents.

Solvent	λ_{abs}/nm	$FWHW_{abs}$/nm	$Area_{abs}$	λ_{em}/nm	$\Delta\lambda$/nm	φ	ε/L mol^{-1} cm^{-1}
Toluene	354/409	120	4.06	515	106	0.450	7230
$CHCl_3$	362/412	138	6.62	550	138	0.270	10,144
DCM	363/413	118	4.80	558	145	0.330	8492
EA	358/408	117	4.50	539	131	0.320	8244
ACN	362/415	117	4.58	580	165	0.180	8278
DMF	366/416	121	4.61	576	160	0.230	7998
DMSO	368/416	130	5.96	589	173	0.160	9618
EtOH	369/413	111	4.82	605	225	0.014	8824
MeOH	376/413	115	5.45	615	202	0.006	9114
H_2O	391/414	98	4.27	652	238	0.002	8494
DMSO–d_6	367/420	121	3.58	589	169	0.110	6260
CD_3OD	370/412	114	4.95	615	203	0.008	8654
D_2O	387/414	102	5.11	608	194	0.011	9940

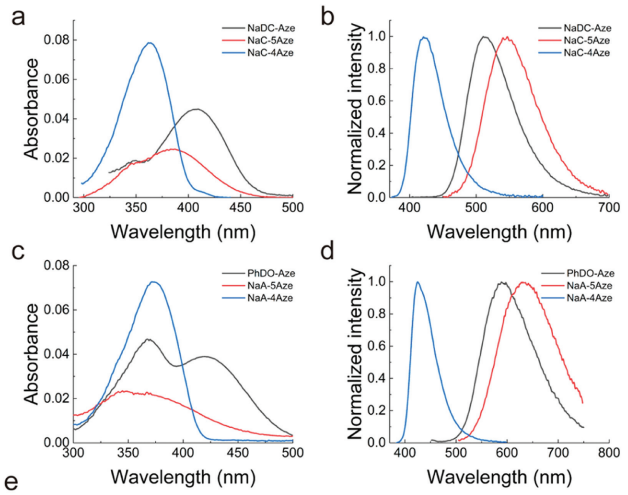

e

Compounds	λ_{abs}/nm	$FWHW_{abs}$ /nm	$Area_{abs}$	λ_{em}/nm	Δλ/nm	φ	ε /L mol^{-1} cm^{-1}
NaDC-Aze	410	77	3.87	511	101	0.75	8992
NaC-5Aze	383	88	2.14	554	171	0.56	4951
NaC-4Aze	362	53	4.46	421	59	0.26	15777
PhDO-Aze	368/416	122	5.38	589	173	0.16	9618
NaA-5Aze	350	106	2.68	628	278	0.053	4471
NaA-4Aze	373	59	4.52	426	53	0.068	17508

Fig. 1. Characterization of the spectral properties of fluorophores. (a) UV–vis absorption spectra and (b) normalized fluorescence spectra of **NaDC-Aze** (Ex: 390 nm), **NaC-5Aze** (Ex: 360 nm), and **NaC-4Aze** (Ex: 360 nm) in DMSO. (c) UV–vis absorption spectra and (d) normalized fluorescence spectra of **PhDO-Aze** (Ex: 400 nm), **NaA-5Aze** (Ex: 350 nm), and **NaA-4Aze** (Ex: 370 nm) in DMSO. (e) Photophysical data of the six compounds. Dye concentrations: 5 μmol/L.

of the two parent dyes, accompanied by higher fluorescence quantum yields compared to those of the parent dyes.

These "superimposed" spectral properties are likely the results of the hybridization within the cross-conjugation systems in **NaDC-Aze** and **PhDO-Aze**. Specifically, the presence of two absorption peaks in the absorption spectra, along with the intermediate absorption intensity, indicates the coexistence of two electron-delocalization systems in a cross-conjugation manner in both **NaDC-Aze** and **PhDO-Aze**. Upon light absorption and transition to the excited states, the delocalized system of the **NaC/Nac-4Aze**-type exhibits a high-energy level. Subsequently, internal conversion towards the lower-energy delocalized system of the **NaC/NaA-5Aze**-type results in the emission of long-wavelength fluorescence.

We further performed quantum chemical calculations to substantiate the experimental data (Fig. 2). Our calculations show that dye **NaC-5Aze** exhibits a lower optical gap (3.502 eV) compared to dye **NaC-4Aze** (3.833 eV), attributable to significantly enhanced intramolecular charge transfer (ICT) [24,25]. For instance, the calculated charge transfer distance, or the centroid distance between the hole and the electron, measures 2.19 Å for **NaC-5Aze** and 0.77 Å for **NaC-4Aze**. This pronounced ICT in **NaC-5Aze** justifies its redshift relative to **NaC-4Aze**. Additionally, the stronger ICT in **NaC-5Aze** results in a lower oscillator strength ($f = 0.25$), consequently leading to a reduced molar extinction coefficient. Conversely, despite its blue shifts, **NaC-4Aze**'s reduced degree of ICT results in a higher oscillator strength ($f = 0.50$), explaining its large molar extinction coefficient. These findings align well with experimental observations. We also noted that the S_2 state of both **NaC-5Aze** and **NaC-4Aze** show small oscillator strength, indicative of weak absorbance.

Interestingly, the cross-conjugated hybrid dye **NaDC-Aze** exhibits an electronic and spectral structure "superimposable" on those of its parent dyes **NaC-5Aze** and **NaC-4Aze**. The S_1 optical gap of **NaDC-Aze** (3.484 eV) is remarkably similar to that of

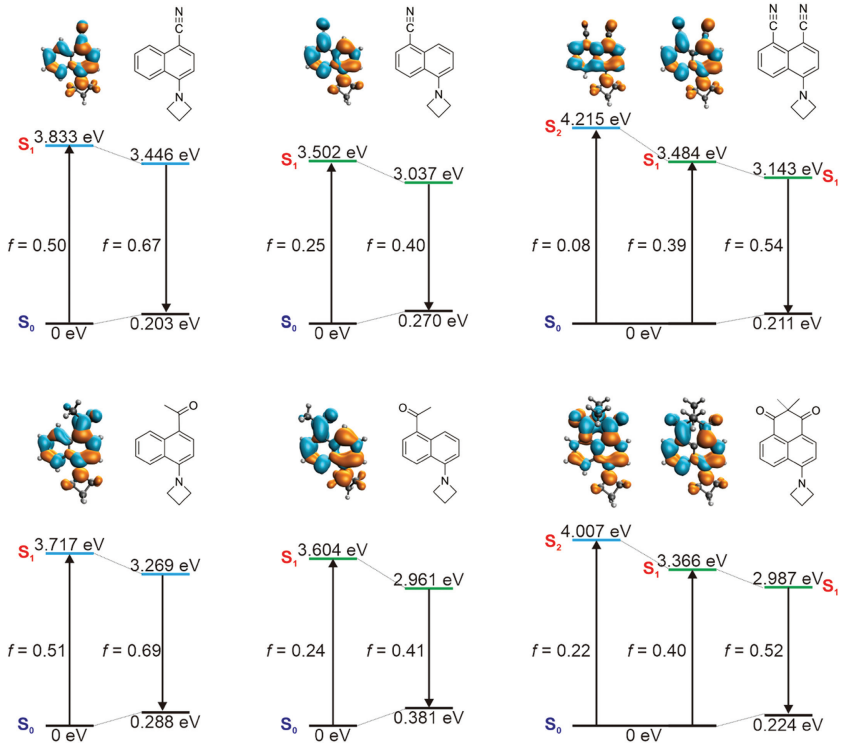

Fig. 2. Calculated optical gaps during the UV–vis absorption and emission processes of **NaC-4Aze**, **NaC-5Aze**, **NaDC-Aze** (the top panel), **NaA-4Aze**, **NaA-5Aze**, and **PhDO-Aze** (the bottom panel). The insets show the molecular structures, oscillator strengths, and electron/hole plots during the vertical excitation of these dyes. Green: electron; orange: hole.

NaC-5Aze (3. 502 eV). The charge distribution analysis reveals that in **NaDC-Aze**, charge predominantly migrates towards the electron-withdrawing group at the 5-position. The atomic contribution at the 5-position substituent in the lowest unoccupied molecular orbital (LUMO) of **NaDC-Aze** amounts to ~0.09, in contrast to the 4-position substituent which is only ~0.02. This difference mirrors the strong ICT effect observed in **NaC-5Aze** when an electron-withdrawing group is present at the 5-position, attracting charge density upon photoexcitation. Additionally, **NaDC-Aze** possesses a bright S_2 state ($f = 0.08$) with π-π transition characteristics, leading to the manifestation of two absorption peaks within the first absorption band, corroborating experimental data.

However, the spectral characteristics of **NaDC-Aze** do not merely represent an additive combination of those of **NaC-5Aze** and **NaC-4Aze**. During S_1 photoexcitation of **NaDC-Aze**, the 4-position substituents also engage in π-conjugation, although their charge density shift is less pronounced than that of the 5-position substituents. The charge transfer distance (d_{CT}) during the S_1 photoexcitation of **NaDC-Aze** is calculated to be 1.53 Å, resulting in a moderate oscillator strength ($f = 0.39$), positioning it between **NaC-5Aze** ($f = 0.25$) and **NaC-4Aze** ($f = 0.50$). Consequently, the molar extinction coefficient of **NaDC-Aze** at the first UV–vis absorption peak lies between those of **NaC-5Aze** and **NaC-4Aze**. Furthermore, the electron distribution in the S_2 state of **NaDC-Aze** shows enhanced intramolecular charge transfer in comparison to the S_1 state of **NaC-4Aze**. For instance, upon photoexcitation to the S_2 state, the amino donor group in **NaDC-Aze** exhibits a reduced charge density compared to the charge density of **NaC-4Aze**'s amino donor group when excited to the S_1 state (Fig. S21 in Supporting information). These distinctions lead to the S_2 peak absorbance in **NaDC-Aze** ($f = 0.08$) not being as pronounced as the S_1 peak absorbance ($f = 0.50$) in **NaC-4Aze**.

Similar calculations performed on **NaA-5Aze**, **NaA-4Aze**, and **PhDO-Aze** yield analogous results. While the S_1 states of **NaA-5Aze** and **NaA-4Aze** are bright, their S_2 states are almost dark ($f < 0.05$). The cross-conjugation hybrid **PhDO-Aze**, however, exhibits both S_1 and S_2 as bright states with substantial absorbance ($f > 0.20$), with peak wavelengths closely resembling the S_1 of **NaA-5Aze** and **NaA-4Aze**, respectively. Nevertheless, the participation of both electron-withdrawing groups in π-conjugation within **PhDO-Aze**, unlike in **NaA-5Aze** and **NaA-4Aze**, modifies the degree and extent of charge transfer, leading to spectral properties that echo those of **NaA-5Aze** and **NaA-4Aze**, yet are not a straightforward summation.

Due to the inherent environmental sensitivity of **PhDO-Aze**, it serves as a fluorogenic probe for wash-free imaging. Before employing the probe for imaging experiments in live cells, we initially assessed its cytotoxicity using the MTT assay. The cell viability test, conducted after incubating cells with various concentrations of **PhDO-Aze** for 24 h, indicated minimal impact on cell viability (Fig. S2 in Supporting information). Calculated log*P* (Clog*P*) is used to define the lipophilicity of compounds. And "Clog*P* < 5" is considered as strong lipophilicity for lipid droplet imaging. The calculated Clog*P* of **PhDO-Aze** is 3.06, indicating appropriate lipophilicity (Fig. 3a). Based on our prior research [14,26-28], we infer that

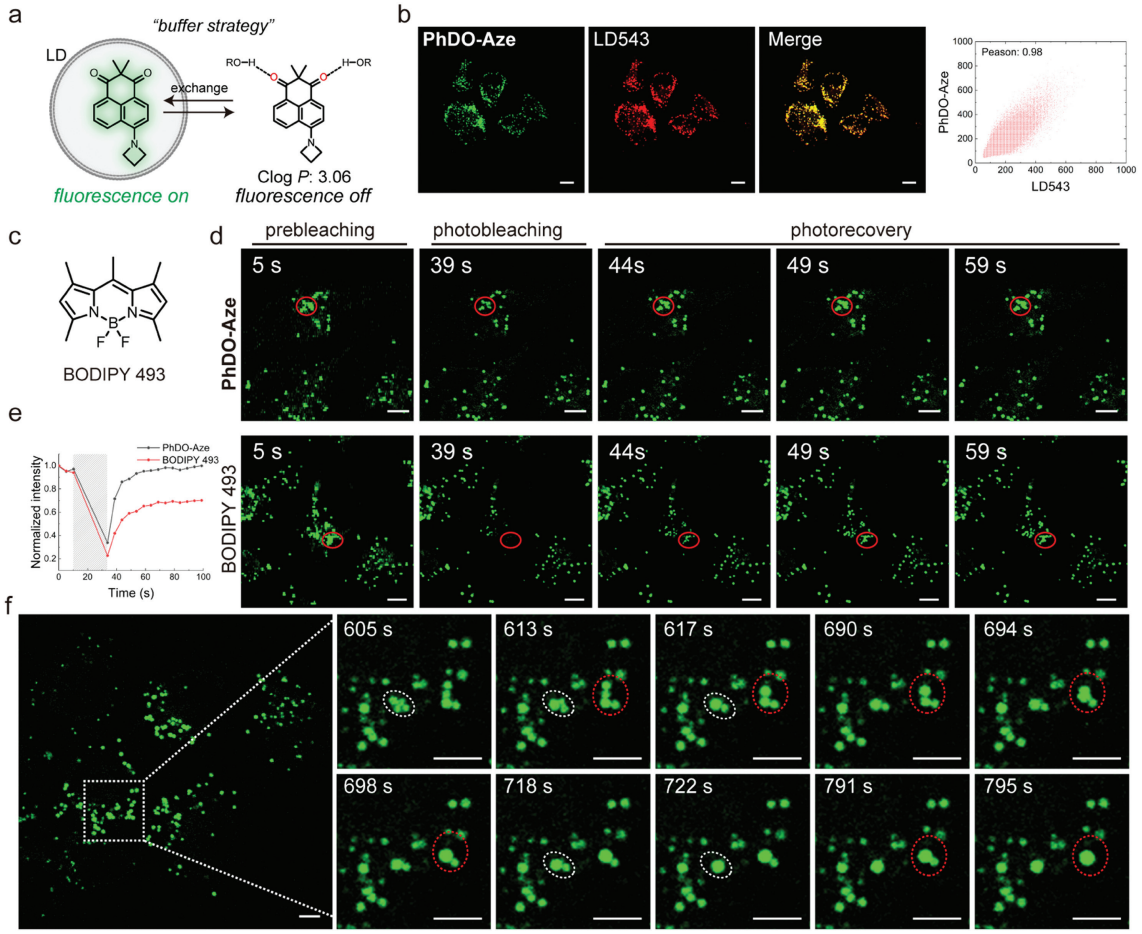

Fig. 3. Fluorogenic imaging of lipid droplets (LD) in live cells using **PhDO-Aze** based on the buffering strategy. (a) Mechanism for LD fluorogenic and dynamic imaging using **PhDO-Aze**. (b) Confocal images of HeLa cells using 1 μmol/L **PhDO-Aze** and 500 nmol/L LD 543. (c) The chemical structure of BODIPY 493. (d) Confocal images of live HeLa cells during photobleaching and photorecovery processes using 2 μmol/L **PhDO-Aze** and BODIPY 493. Red circles highlighted the bleaching area. (e) Relative intensity of the bleaching area during the photobleaching and photorecovery processes as shown in (d). (f) Confocal image of live HepG2 cells with 1 μmol/L **PhDO-Aze** and the locally enlarged images of the boxed region for dynamic LD coalescence. Scale bar: 5 μm.

it is an excellent buffering probe suitable for lipid droplet imaging. Through co-localization experiments, the Pearson correlation coefficient (PCC) between **PhDO-Aze** and LD 543, a commercial lipid droplet dye, was calculated to be 0.96 (Fig. 3b). This high PCC value indicates that **PhDO-Aze** has strong targeting ability to lipid droplets. Furthermore, we investigated the buffering capability of the probe through fluorescence recovery after photobleaching (FRAP) experiments. We found that **PhDO-Aze** rapidly recovered to its initial fluorescence intensity within 20 s post-photobleaching, while BODIPY 493, a commercial lipid droplet dye, exhibited a slower recovery rate, reaching only 60% of the initial fluorescence intensity (Figs. 3c–e). Subsequently, we employed confocal imaging to observe the dynamic behavior of lipid droplets in HepG2 cells using **PhDO-Aze**. Imaging results showed that multiple lipid droplets fused into one larger lipid droplet multiple times within 3 min (Fig. 3f). These results indicate that **PhDO-Aze** is an outstanding lipid droplet buffering probe. Owing to its substantial Stokes shift, **PhDO-Aze** can also serve as a powerful tool for multi-color imaging of cellular organelles, revealing additional physiological functions of lipid droplets.

In this paper, we utilize naphthalene fluorophores, **NaDC-Aze** and **PhDO-Aze**, as a case study to underscore the crucial role of cross-conjugation in the structure-property relationship of fluorophores. Formed by hybridizing two distinct conjugated systems within a single naphthalene molecule, **NaDC-Aze** and **PhDO-Aze** showcase spectral characteristics from both conjugated parent systems. Both experimental data and theoretical calculations support the presence and function of two coexisting electron delocalization systems in a cross-conjugation manner within **NaDC-Aze** and **PhDO-Aze**, affording broad absorption bands, bright fluorescence, and large Stokes shifts. This work is anticipated to offer a fresh perspective on understanding the structure-property relationships of fluorophore structures and contribute to the development of novel fluorophores in the future.

Declaration of competing interest

The authors declare that they have no known competing financial interests or personal relationships that could have appeared to influence the work reported in this paper.

CRediT authorship contribution statement

Kai An: Data curation, Writing – original draft. **Qinglong Qiao:** Supervision. **Lovelesh:** Data curation. **Syed Ali Abbas Abedi:** Data curation. **Xiaogang Liu:** Data curation, Writing – review & editing. **Zhaochao Xu:** Conceptualization, Funding acquisition, Supervision, Writing – original draft, Writing – review & editing.

Acknowledgments

This work is supported by the National Natural Science Foundation of China (Nos. 22225806, 22078314, 21908216, 22378385) and Dalian Institute of Chemical Physics (Nos. DICPI202142, DICPI202436), Agency for Science, Technology and Research (No. A*STAR, Singapore) under its Advanced Manufacturing and Engineering Program (No. A2083c0051), and SUTD Kickstarter Initiative (No. SKI 2021_03_10). The authors are grateful for the supercomputing resources of SUTD-MIT IDC and the National Supercomputing Centre (Singapore).

Supplementary materials

Supplementary material associated with this article can be found, in the online version, at doi:10.1016/j.cclet.2024.109786.

References

[1] R.W. Sinkeldam, N.J. Greco, Y. Tor, Chem. Rev. 110 (2010) 2579–2619.
[2] E.M.S. Stennett, M.A. Ciuba, M. Levitus, Chem. Soc. Rev. 43 (2014) 1057–1075.
[3] A. Kurutos, D. Citterio, J. Mol. Struct. 1247 (2022) 131381.
[4] J.V. Jun, E.J. Petersson, D.M. Chenoweth, J. Am. Chem. Soc. 140 (2018) 9486–9493.
[5] M. Pengshung, P. Neal, T.L. Atallah, et al., Chem. Commun. 56 (2020) 6110–6113.
[6] C.X. Yan, Z.Q. Guo, W.J. Chi, et al., Nat. Commun. 12 (2021) 3869.
[7] C.S. Abeywickrama, Chem. Commun. 58 (2022) 9855–9869.
[8] X. Cheng, S. Huang, Q. Lei, et al., Chin. Chem. Lett. 33 (2022) 1861–1864.
[9] W. Chi, Q. Qiao, C. Wang, et al., Angew. Chem. Int. Ed. 59 (2020) 20215–20223.
[10] X.G. Liu, Q.L. Qiao, W.M. Tian, et al., J. Am. Chem. Soc. 138 (2016) 6960–6963.
[11] Z.G. Yang, A. Sharma, J. Qi, et al., Chem. Soc. Rev. 45 (2016) 4651–4667.
[12] C.Y. Li, G.C. Chen, Y.J. Zhang, et al., J. Am. Chem. Soc. 142 (2020) 14789–14804.
[13] Q.L. Qiao, W.J. Liu, J. Chen, et al., Angew. Chem. Int. Ed. 61 (2022) e202202961.
[14] J. Chen, W.J. Liu, X.N. Fang, et al., Chin. Chem. Lett. 33 (2022) 5042–5046.
[15] J.J. Yim, S. Harmsen, K. Flisikowski, et al., Proc. Natl. Acad. Sci. U. S. A. 118 (2020) e2008072118.
[16] X. Zhao, Q.C. Yao, S. Long, et al., J. Am. Chem. Soc. 143 (2021) 12345–12354.
[17] C.E. Yang, H.R. Wang, S. Yokomizo, et al., Angew. Chem. Int. Ed. 60 (2021) 13847–13852.
[18] W.J. Liu, J. Chen, Q.L. Qiao, et al., Chin. Chem. Lett. 33 (2022) 4943–4947.
[19] Z.F. Li, Q.L. Qiao, N. Xu, et al., Chin. Chem. Lett. 35 (2024) 108824.
[20] J. Li, Q.L. Qiao, Y.Y. Ruan, et al., Chin. Chem. Lett. 34 (2023) 108266.
[21] J.P. Ding, R.S. Xiao, A.Y. Bi, et al., Chin. Chem. Lett. 34 (2023) 108273.
[22] T. Beppu, K. Tomiguchi, A. Masuhara, et al., Angew. Chem. Int. Ed. 54 (2015) 7332–7335.
[23] H. John, C. Briehn, J. Schmidt, et al., Angew. Chem. Int. Ed. 46 (2007) 449–453.
[24] X. Wu, D. Tan, Q.L. Qiao, et al., Phys. Chem. Chem. Phys. 24 (2022) 15937–15944.
[25] X.G. Liu, J.M. Cole, Z.C. Xu, J. Phys. Chem. C 121 (2017) 13274–13279.
[26] J. Chen, C. Wang, W.J. Liu, et al., Angew. Chem. Int. Ed. 60 (2021) 25104–25113.
[27] W. Zhou, Q.L. Qiao, Y. Tao, et al., Sens. Actuat. B: Chem. 376 (2023) 132980.
[28] N. Xu, Q.L. Qiao, J. Chen, et al., Chem. Commun. 60 (2024) 1424–1427.